Graphene–Polymer Hybrid Nanostructure-Based Bioenergy Storage Device for Real-Time Control of Biological Motor Activity

Kyung-Eun Byun,[†] Dong Shin Choi,[‡] Eunji Kim,[§] David H. Seo,[⊥] Heejun Yang,[⊥] Sunae Seo,[⊥,∥] and Seunghun Hong[†,‡,§,*]

[†]Department of Physics and Astronomy, [‡]Department of Nano Science and Engineering, and [§]Department of Biophysics and Chemical Biology, Seoul National University, Seoul, 151-742 Korea, [⊥]Graphene Research Center, SAIT Samsung Research Park, Yongin-Si, Gyeonggi-Do, 446-712 Korea, and [∥]Department of Physics, Sejong University, Seoul, 143-747 Korea

ABSTRACT

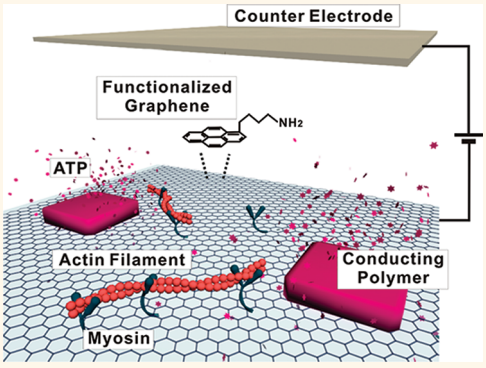

We report a graphene–polymer hybrid nanostructure-based bioenergy storage device to turn on and off biomotor activity in real-time. In this strategy, graphene was functionalized with amine groups and utilized as a transparent electrode supporting the motility of biomotors. Conducting polymer patterns doped with adenosine triphosphate (ATP) were fabricated on the graphene and utilized for the fast release of ATP by electrical stimuli through the graphene. The controlled release of biomotor fuel, ATP, allowed us to control the actin filament transportation propelled by the biomotor in real-time. This strategy should enable the integrated nanodevices for the real-time control of biological motors, which can be a significant stepping stone toward hybrid nanomechanical systems based on motor proteins.

KEYWORDS: biomotor · actin filament · myosin · graphene · conducting polymer · polypyrrole

Biological motors can generate force and motion in living systems using the chemical energy of adenosine triphosphate (ATP) molecules as a fuel. Since these motor proteins are much smaller in size and better in fuel efficiency compared to any man-made motors, they have been drawing attention as a key component for highly efficient nanomechanical systems.[1−3] For such nanomechanical systems based on motor protein, it is crucial to control the motility of the motor protein in real-time. Many researchers have tried to control the activity of motor proteins utilizing various methods such as microfluidics[4−7]or UV-active compounds.[8−10] However, the method based on microfluidics required extra steps such as buffer exchange and could not be used for local control of biomotor motility.[4−7] In the case of the DMNPE-caged ATP method, the initial concentration was limited to ~0.5 mM because the DMNPE-caged ATP molecules acted as a competitive inhibitor for motor protein.[8−10] Also, one should be cautious in minimizing the illumination to avoid unwanted release of caged ATP.[8−10] These strategies based on microfluidics or caged ATP can efficiently turn on or off the biomotor activity by controlling chemical environments, but they require bulky systems which could not be integrated into compact devices for nanomechanical systems. As a solution for such device integration, electrical control methods have been studied to control the motor protein motions. However, previous electrical control methods often suffered from various limitations such as slow response in on/off cyclic control,[11] poor on/off ratio,[12] and a lack of localized-control capability.[13,14] On the other hand, graphene has been drawing attention as a possible electrical component for biological applications[15,16] due to its exotic properties such as chemical stability, high conductivity, high flexibility, and good transparency.[17,18] However, the motility of motor protein on graphene has not been demonstrated yet. Herein, we developed a

* Address correspondence to seunghun@snu.ac.kr.

Received for review June 30, 2011 and accepted October 21, 2011.

Published online October 21, 2011
10.1021/nn202421n

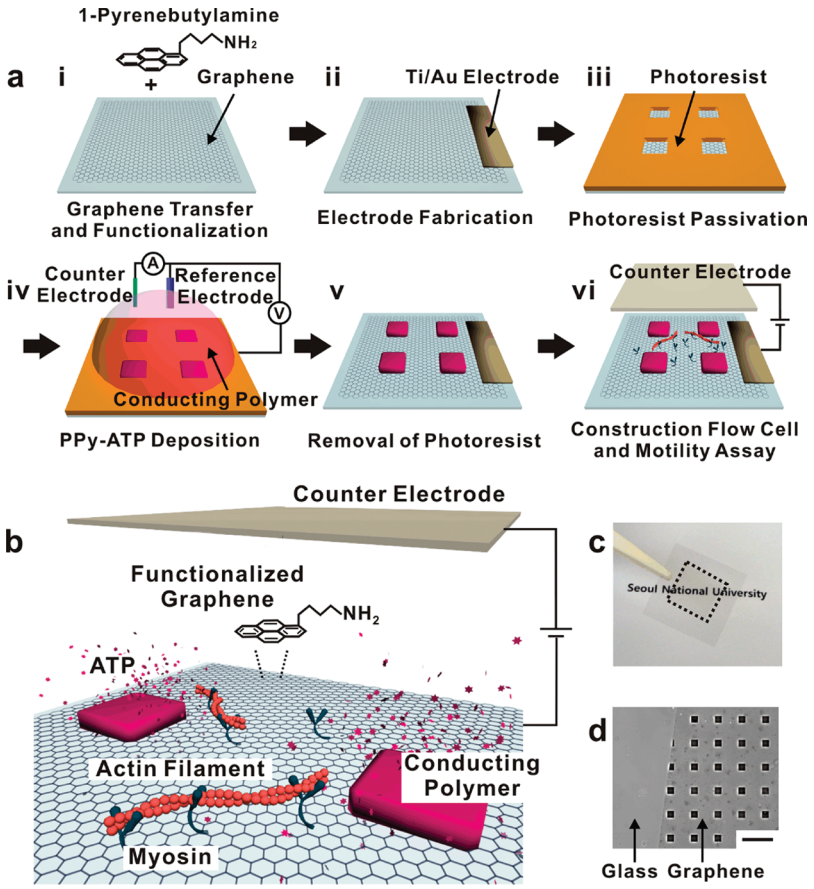

Figure 1. Graphene–polymer hybrid nanostructures for the real-time control of biological motors. (a) Schematic diagram depicting the fabrication procedure of a graphene–polymer hybrid device and *in vitro* motility assay on the device. (i) Graphene transfer and functionalization. The graphene layer transferred onto a glass substrate was functionalized with amine groups by coating it with 1-pyrenebutylamine. (ii) Deposition of a Ti/Au electrode by thermal evaporation through a shadow mask. (iii) Fabrication of photoresist patterns on the graphene substrate *via* photolithography. (iv) Electrochemical deposition of ATP-doped conducting polymer (PPy-ATP). Photoresist prevents the deposition of conducting polymer. (v) Removal of photoresist. (vi) *In vitro* motility assay on the device. (b) Schematic diagram depicting the real-time control of the motility of actomyosin utilizing a graphene–polymer hybrid device. (c) Optical image of transparent graphene on a glass substrate. The black dotted square indicates the region covered by graphene. (d) Optical micrograph of PPy-ATP patterns on the graphene substrate. The square-shaped black regions represent PPy-ATP patterns.

graphene–polymer hybrid nanostructure-based bioenergy storage device which allowed us to switch the biomotor activity between on-and-off states in real-time. In this strategy, conducting polymer patterns containing ATP, as fuel storage, were prepared *via* photolithography on amine-functionalized graphene substrates. The amine-functionalized graphene surface supported the motor protein motion with the motility even higher than conventional substrates such as a glass substrate coated with nitrocellulose. ATP molecules were released from the conducting polymer patterns by an electrical stimulus through graphene, which successfully activated motor protein motility. As a proof of concept, we demonstrated the repeated activation and deactivation of motor protein activities by electrical stimuli in the media with hexokinase which depleted remaining ATP. This result is the first demonstration of the motor protein-induced transportation of the actin filaments on graphene and the real-time control of the motility using the integrated fuel supply device. Since our method does not use high-temperature processing steps or any unconventional fabrication method, *graphene–polymer hybrid devices* can be an ideal strategy for integrated hybrid nanomechanical systems based on motor protein.

RESULTS AND DISCUSSION

Figure 1a shows a schematic diagram depicting the fabrication procedure of our graphene–polymer hybrid device. We fabricated ATP-doped polypyrrole (PPy-ATP) patterns on a functionalized graphene substrate for a bioenergy storage device. The doped conducting polymers on conventional metallic electrodes have been utilized for the controlled release of bioactive chemicals[19–23] and the control of rather *slow* processes such as cell growth.[24,25] The detailed procedure for our fabrication method for ATP-doped polypyrrole patterns on graphene can be found in the Materials and Methods section. Briefly, multilayered graphene grown by chemical vapor deposition (CVD)

was transferred onto a glass substrate. Then, the graphene substrate was functionalized with amine groups by immersing it in a 1-pyrenebutylamine solution (Figure 1a(i)). In the solution, the 1-pyrenebutylamine adhered to the graphene surface *via* $\pi-\pi$ interaction.[26,27] After the functionalization, a Ti/Au electrode was deposited *via* thermal evaporation (Figure 1a(ii)). Next, a photoresist was patterned on the graphene substrate *via* photolithography (Figure 1a(iii)). PPy-ATP films were then synthesized from the mixture of pyrrole and ATP aqueous solution by the electrochemical deposition method (Figure 1a(iv)).[20] Note that the polypyrrole was deposited only on the exposed graphene regions since the photoresist pattern worked as a passivation layer. During the deposition process, negatively charged ATP molecules were incorporated into polypyrrole to stabilize the positively charged backbone of polypyrrole. Finally, the photoresist was removed by acetone (Figure 1a(v)), resulting in graphene–polymer hybrid structures for a controlled *in vitro* motility assay (Figure 1a(vi)). Note that this process can be done at rather low temperature using only conventional microfabrication facilities, and thus it is readily accessible to present device manufacturing.

Figure 1b shows a schematic diagram depicting the real-time control of motor protein utilizing the graphene–polymer hybrid device. For the *in vitro* motility assay of motor protein, we used actin filaments and myosin (actomyosin), one of the linear motor protein systems.[28] The detailed procedure of the *in vitro* motility assay on the graphene–polymer hybrid device can be found in the Materials and Methods section. Briefly, the graphene–polymer hybrid device was first incubated with heavy meromyosin (HMM) which was produced from a full-length myosin II protein isolated from rabbit skeletal muscle. HMM consists of the myosin head subfragment-1 (S1), including two light chains, and the coiled-coil subfragment-2 (S2) and has a motor activity. Bovine serum albumin (BSA) was then infused into the device to prevent the nonspecific adsorption of actin filaments.[29] Rhodamine phalloidin-labeled actin filaments were infused into the device, followed by the motility buffer (3 mg·mL^{-1} D-glucose, 50 units·mL^{-1} glucose oxidase, 52 units·mL^{-1} catalase in actin buffer). The labeled actin filaments were observed *via* fluorescence microscopy. The functionalized graphene substrate was utilized as a transparent electrode for the observation of fluorescence-labeled actin filaments and the stimulation of PPy-ATP patterns. When a negative bias voltage was applied to the PPy-ATP patterns through the graphene, the PPy-ATP patterns were stimulated, and the incorporated ATP molecules were released from the PPy-ATP patterns.[20,22] These electrochemically released ATP molecules provided chemical energy to the actomyosin system. Note that the dimension of PPy-ATP patterns with graphene electrodes can be readily scalable, and thus they can be easily integrated into compact devices for nanomechanical systems in the future. Furthermore, since, in this strategy, the electrical stimuli was utilized to control the ATP release rather than to directly affect the motor protein, we can expect rather low damages onto the motor protein.

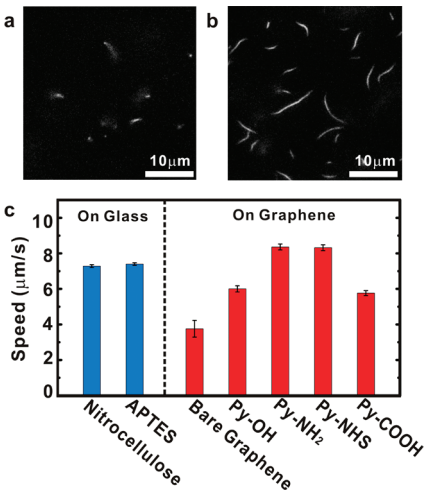

Figure 2. Transportation of actin filaments induced by motor proteins on functionalized graphene surfaces. (a) Fluorescence micrograph of actin filaments on a bare graphene surface. (b) Fluorescence micrograph of actin filaments on an amine-functionalized graphene surface. (c) Graph showing the average speed of actin filaments on conventional substrates (a glass substrate coated with nitrocellulose or 3-aminopropyltriethoxysilane (APTES)) and various graphene substrates functionalized with 1-pyrenebutanol (Py-OH), 1-pyrenebutyl amine (Py-NH_2), 1-pyrenebutyric acid *N*-hydroxysuccinimide ester (Py-NHS), or 1-pyrenebutyric acid (Py-COOH). The error bars represent the standard errors of the mean from the data. Note that the motility on the amine- or the NHS-functionalized graphene was as high as that on the conventional substrates.

Figure 1c shows an optical image showing the transparency of graphene on a cover glass. The black dotted square represents the graphene area whose transparency appeared similar to that of the glass area. Note that the underlying letters could be seen through the transparent graphene. The transparency of our graphene within the visible region (380–770 nm) was measured as 94.9% (Figure S1 in Supporting Information).[30] The excellent transparency of graphene allowed us to observe fluorescence-labeled actin filaments well through the graphene.

Figure 1d shows the optical micrograph of PPy-ATP patterns on a graphene substrate. Numerous PPy-ATP patterns (square-shaped black regions) were uniformly distributed over the large graphene area. The graphene region between the PPy-ATP patterns appeared as transparent as the glass region. In our strategy, large-scale graphene worked as a transparent electrode, so we could stimulate all PPy-ATP patterns over a large area through the graphene without any additional interconnection.

To utilize graphene for nanomechanical systems based on motor protein, graphene should support actomyosin motility well. We performed an *in vitro*

actomyosin motility assay on a graphene surface. Figure 2a shows the fluorescence micrograph of actin filaments on a bare graphene surface (see Supporting Information movie S1). In the case of bare graphene, most of the actin filaments were floating in the solution without interacting with myosin. Only a few actin filaments moved on the bare graphene surface, but they soon detached from the surface. It indicates that the bare graphene could not support actomyosin motility well. Similar behavior has been found from the actomyosin system on carbon nanotube networks as we reported previously.[31] Presumably, protein shows bad adhesion on superhydrophobic surfaces such as graphene and carbon nanotubes,[32−34] although myosin adhered well to moderately hydrophobic surfaces.[35]

To improve actomyosin motility, graphene was functionalized with various molecular species such as 1-pyrenebutanol (Py-OH), 1-pyrenebutyl amine (Py-NH_2), 1-pyrenebutyric acid *N*-hydroxysuccinimide ester (Py-NHS), or 1-pyrenebutyric acid (Py-COOH). Then, we performed the motility assay on these differently functionalized graphene surfaces. Figure 2b shows the fluorescence micrograph of actin filaments interacting with myosin on Py-NH_2-functionalized graphene (see Supporting Information movie S1). Most of the actin filaments bound well to myosin on the functionalized graphene surface and exhibited good motility. We confirmed that the number of actin filaments increased on functionalized graphene compared to bare graphene. The results show that the functionalization of graphene enhanced the adhesion and the motility of actomyosin.

We analyzed the motility of actomyosin on the functionalized graphene surfaces (Figure 2c). Conventional glass substrates coated with nitrocellulose or 3-aminopropyltriethoxysilane (APTES) were utilized as reference surfaces. The average speed of actin filaments on the glass substrate coated with nitrocellulose or APTES was 7.3 ± 0.1 $\mu m \cdot s^{-1}$ (n = 123) or 7.4 ± 0.1 $\mu m \cdot s^{-1}$ (n = 121), respectively. The error bars represent the standard error of the mean from the data. The motility on the bare graphene surface was 3.8 ± 0.5 $\mu m \cdot s^{-1}$ (n = 19). On the other hand, the average speed of actin filaments on the graphene substrate functionalized with Py-OH, Py-NH_2, Py-NHS, or Py-COOH was 6.0 ± 0.2 $\mu m \cdot s^{-1}$ (n = 84), 8.4 ± 0.2 $\mu m \cdot s^{-1}$ (n = 99), 8.3 ± 0.2 $\mu m \cdot s^{-1}$ (n = 158), or 5.8 ± 0.1 $\mu m \cdot s^{-1}$ (n = 141), respectively. The actin filaments on the functionalized graphene surfaces moved faster than those on the bare graphene. Moreover, the actomyosin motility on the amine- or NHS-functionalized graphene substrate was comparable or even higher compared with that on the control substrate such as a nitrocellulose- or APTES-coated glass substrate. We would like to point out that this is the first demonstration of the motor-induced actin filament transportation on graphene. We also analyzed the motility of actomyosin on the functionalized graphene surfaces with different temperatures of 25, 27.5, and 30 °C. In this temperature range, the gliding speeds of the actin filaments were also found to be higher on the amine- or NHS-functionalized graphene substrates than those on the bare graphene surface (Figure S2 in Supporting Information). It is also worth mentioning that, for the motility assay in all of our works, graphene substrates were incubated in 1 $mg \cdot mL^{-1}$ HMM solution, that is, a higher HMM concentration than in previous works using glass substrates (Materials and Methods).[29] It was to ensure a good coverage of HMM on graphene substrates whose surface properties related with HMM adsorption was still unknown. However, we also found that graphene surfaces incubated in lower concentration HMM solution also provided a reasonable motility. For example, when a NH_2-functionalized graphene substrate incubated in 1 $mg \cdot mL^{-1}$ HMM solution exhibited 8.7 $\mu m \cdot s^{-1}$ (n = 24), a similar NH_2-functionalized graphene substrate incubated in 0.1 $mg \cdot mL^{-1}$ HMM solution had 6.5 $\mu m \cdot s^{-1}$ (n = 19) under the same conditions.

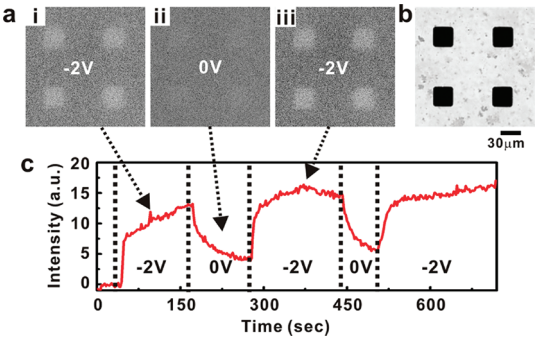

Figure 3. Bioluminescence assay showing the release of ATP from PPy-ATP patterns. (a) Luminescence micrographs of a graphene−polymer hybrid device when −2 V was applied (i,iii) or when the voltage was turned off (ii). (b) Optical micrograph of the graphene−polymer hybrid device. The black square-shaped regions represent PPy-ATP patterns. (c) Graph showing the bioluminescence intensity with different bias voltages onto the graphene substrate. The bioluminescence intensity was averaged over four square-shaped PPy-ATP regions. The luminescence intensity indicating ATP molecules was repeatedly increased and decreased by electrical stimuli.

A plausible explanation for different motilities on functionalized graphene surfaces can be the hydrophobicity and charges on the graphene surfaces.[36] Previous works show that the motility of actomyosin was significantly reduced on hydrophobic surfaces with its contact angle larger than 80°.[37] The contact angles of bare, OH-functionalized, NH_2-functionalized, NHS-functionalized, and COOH-functionalized graphene surfaces were measured as 88, 83, 80, 74, and 81°, respectively (Table S1 in Supporting Information). Thus, the rather poor motility of our bare graphene surfaces can be explained by the large contact angle or hydrophobicity of the bare graphene surfaces. On the other hand, NH_2- or NHS-functionalized graphene surfaces exhibited a rather high mobility of actomyosin, which can be attributed to the reduced hydrophobicity of those graphene surfaces compared

with graphenes with other functionalization. Furthermore, it was reported previously that positive charges on the substrate enhanced the motility of actomyosin.[38] Thus, the positive charges on NH_2- or NHS-functionalized graphene surfaces should have been advantageous for a high motility compared with other graphene surfaces.

We confirmed the release of ATP from a graphene−polymer hybrid device *via* bioluminescence assay (Figure 3). The mixture of luciferin and luciferase is often used to indicate ATP molecules.[23] Luciferin is rapidly oxidized by luciferase in the presence of ATP, producing light. Thus, we can confirm the release of ATP by observing the luminescence from luciferin−luciferase reaction. Panels a and b of Figure 3 are the luminescence micrographs at different bias voltages and the optical micrograph of the graphene−polymer hybrid device, respectively. The four square-shaped dark regions in the optical micrograph represent PPy-ATP patterns. The size of the PPy-ATP pattern was 30 μm × 30 μm, and the space between the patterns was 70 μm. When a negative bias voltage of −2 V (*vs* the counter electrode) was applied to the graphene−polymer hybrid device, the regions of the PPy-ATP patterns became brighter (Figure 3a(i,iii)). The bright regions in the luminescence micrographs and the PPy-ATP patterns in the optical micrograph were matched well. With a zero bias voltage, the luminescence in the PPy-ATP regions faded away (Figure 3a(ii)). This result implies that the incorporated ATP molecules were released from the PPy-ATP patterns with the negative bias voltage, but they were not released after turning off the voltage.

Figure 3c shows the averaged luminescence intensity of the four PPy-ATP regions as time passed. The luminescence intensity was repeatedly increased or decreased, and it coincided with the electrical stimuli. The PPy-ATP patterns released ATP molecule whenever we applied the bias voltage, and the patterns stopped releasing ATP when we turned off the bias voltage. The remaining ATP in the buffer solution was consumed by the luciferase as time passed, thus the luminescence intensity decreased slowly. It should be noted that the ATP molecules were repeatedly released from the graphene−polymer hybrid structures by the electrical stimuli.

We estimated how much ATP can be stored in each PPy-ATP pattern and can be released from it. The detailed explanation can be found in Supporting Information (supplementary note 1, Figure S3, and Figure S4a). In brief, the initial ATP concentration within a PPy-ATP pattern was estimated as 1.7 M. Then, ATP release from the PPy-ATP patterns was simulated using a commercial finite element method package, COMSOL Multiphysics. We modeled a graphene−polymer hybrid system based on the thin layer diffusion model.[39] On the basis of the results from the COMSOL simulation, ATP concentration inside the PPy-ATP patch was estimated as 1.70 M at 0 s, 1.69 M at 10 s, and 1.68 M at 20 s during the application of a negative bias voltage (−1 V *vs* the counter electrode) (Figure S4a in Supporting Information). Therefore, 1×10^{-14} mol of ATP was released from each PPy-ATP pattern for each 10 s at the initial stage. Assuming that the ATP in our present PPy-ATP patterns was used up to fill our flow cell with its dimension of 1 cm × 0.8 cm × 150 μm ($W \times L \times H$), the ATP concentration in the flow cell could increase up to 1.02 mM, which is already higher than the maximum ATP concentration limit of ∼0.5 mM by the DMNPE-caged ATP method.[8] However, it also should be noted that the maximum possible ATP concentration by our method can be increased much further simply by using larger-size PPy-ATP patterns, implying that our method can be utilized to control the ATP concentration from zero up to a very high concentration.

We demonstrated the real-time control of actomyosin motility using the graphene−polymer hybrid device (Figure 4). Figure 4a is the time series of fluorescence micrographs showing the activation of actomyosin by electrical stimuli (see Supporting Information movie S2). A PPy-ATP pattern was located in the bottom left of the figure (a red solid line). Before electrical stimuli, actin filaments on myosin did not move at all because there was no ATP in the buffer solution (Figure 4a(i,ii)). When a negative bias voltage (−1 V *vs* the counter electrode) was applied to PPy-ATP patterns through the graphene, actin filaments began to move (Figure 4a(iii,iv)). The trajectory of actin filaments are represented by white dotted lines in Figure 4a(iv). The amount of the released ATP by short-time electrical stimuli (20 s) was enough to maintain actomyosin motility over an hour. Interestingly, actin filaments which were close to the PPy-ATP pattern (white arrows in Figure 4a(iii)) began to move first. It implies that the ATP concentration near the PPy-ATP pattern was initially higher than the other region.

One should be cautious about the stability of actomyosin motility on the graphene−polymer hybrid device because high electrical currents may cause the degradation of protein. During the motility experiments, we mostly applied −1 V bias onto the graphene electrode, while −2 V or higher bias voltage was utilized only for a short time period (<3 s). However, the actomyosin motility did not change even after long-time electrical stimuli (over 3 min), indicating that the degradation of actomyosin by the electrical stimuli was negligible (Figure S5 in Supporting Information). Presumably, since a negative bias voltage was applied to the graphene electrode with myosin, the reactive oxygen species which might have been generated and damage protein should have been repulsed from the electrode, and thus the damage on the myosin might be minimized during our experiment.[40] At the same time, the generation of waste heat should be taken into account. The measured current was ∼300 nA when −1 V (*vs* the

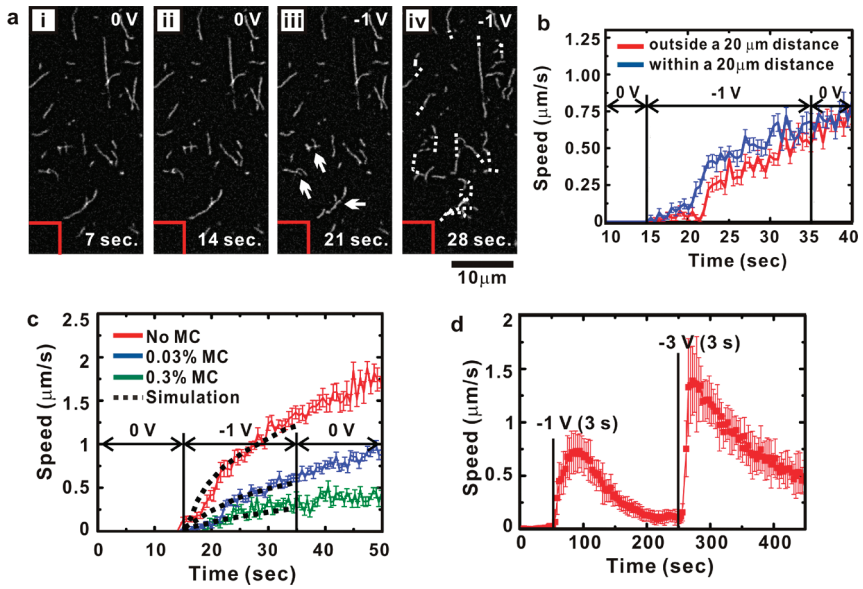

Figure 4. Controlled actomyosin motility utilizing graphene–polymer hybrid nanostructures. (a) Time series of fluorescence micrographs showing controlled actomyosin motility by electrical stimuli. A PPy-ATP pattern was located in the bottom left of the figure (a red solid line). The experiment was performed in a buffer solution with 0.03% methylcellulose (MC). Note that actin filaments did not move before a voltage was applied (i,ii). (iii) Actin filaments close to a PPy-ATP pattern began to move. The moving actin filaments were indicated by white arrows. (iv) Actin filaments in all regions moved. The trajectories were represented by white dotted lines. (b) Graph showing the average speeds of actin filaments in the regions within 20 μm from PPy-ATP patterns and outside of the regions. Blue and red lines represent the speeds of actin filaments in the regions within 20 μm from PPy-ATP patterns and outside of the regions, respectively. (c) Average speeds of actin filaments on a graphene–polymer hybrid device in solutions with different viscosity. Red, blue, and green lines represent the average speed of actin filaments in a buffer solution with no MC, 0.03% MC, and 0.3% MC, respectively. The black dotted lines represent the simulated speed of actin filaments in each case. To calculate the simulation speed, the ATP concentration in the graphene–polymer hybrid device was first obtained from the simulation based on the thin layer diffusion model (Figure S4),[43] and then, the simulated speeds were calculated from the simulated ATP concentration using the measured Michaelis–Menten relationship (Figure S3 in Supporting Information).[44] Note that the speed of actin filaments decreased as the viscosity of the solution increased. (d) Graph showing the repeated activation of actomyosin in a buffer solution without MC. Two different bias voltages (−1 V at 50 s and −3 V at 250 s) were applied to the graphene substrate for 3 s. After actomyosin was activated by the electrical stimuli, the speed of actin filaments was rapidly decreased because hexokinase consumed the released ATP. The actomyosin was repeatedly activated by the electrical stimuli in real-time.

counter electrode) was applied to the graphene electrode. Thus, 3×10^{-7} J·s^{-1} of electric power was generated. Assuming that 100% of the electric power was used for heating the water in the flow cell during the application of the −1 V for 10 s, it can be inferred that the water in the flow cell was heated by only 9.5×10^{-5} °C and therefore the heating effect was negligible.

We analyzed the speed of actin filaments in two different regions: a region within 20 μm from PPy-ATP patterns and outside of this region (Figure 4b). When a bias voltage (−1 V *vs* the counter electrode) was applied to the PPy-ATP patterns through graphene, actin filaments in regions within 20 μm from the PPy-ATP pattern moved first. Moreover, their average speed was higher than that outside of the regions while the voltage was applied. It is because the release of ATP occurred from the PPy-ATP patterns, and the released ATP diffused away from it. Presumably, the speed of actin filaments depends on the concentration of ATP,[41] so the actin filaments which were close to the PPy-ATP moved faster than others.

We demonstrated that the response of our graphene–polymer hybrid device could be regulated by controlling the viscosity of the surrounding media (Figure 4c). In this experiment, methylcellulose (MC) was added to increase the viscosity of the surrounding media. MC has been often used in an *in vitro* motility assay to prevent desorption of actin filaments from a substrate coated with the low density of myosin, while it was known that MC does not affect the motility of actomyosin.[42] Red, blue, and green solid lines in the graph represent the average speed of actin filaments in the buffer solution with no MC, 0.03% MC, and 0.3% MC, respectively. In this case, the gliding speed of actin filament was averaged over the whole regions. When −1 V bias voltage (*vs* the counter electrode) was applied to the PPy-ATP patterns from 15 to 35 s, the biomotor activity was turned on in all cases. For example, without MC, the gliding speed of actin filaments after the electrical stimuli for 20 s was 1.25 μm·s^{-1}, which corresponds to the released ATP concentration of 16.4 μM (Figure 4c and Supporting Information Figure S3). However, actin filaments in the buffer solution with higher viscosity moved more slowly than those in the less viscous solutions. Since MC itself was known not to affect the motility of actomyosin directly,[42] such a difference can be attributed to the slow diffusion of ATP in viscous

buffer solution. Presumably, the high viscosity of the solution slowed the release and the diffusion of ATP molecules from PPy-ATP patterns.

The release of ATP from the graphene–polymer hybrid devices was modeled by the finite element method (supplementary note 1, Figure S3, and Figure S4 in Supporting Information). The black dotted lines in Figure 4c represent the simulated speeds of actin filaments. In this work, the ATP concentration in the graphene–polymer hybrid device was first obtained from the simulation based on the thin layer diffusion model (Figure S4).[43] Then, the simulated speeds of actin filaments were then calculated from the simulated ATP concentration using the measured Michaelis–Menten relationship (Figure S3 in Supporting Information).[44] The simulated speeds of actin filaments and the experimental results coincided well (Figure 4c). It clearly shows that the release of ATP was predictable, and the response of graphene–polymer hybrid devices could be regulated by controlling the viscosity of solutions.

We also demonstrated the repeated activation of actomysoin (Figure 4d and Supporting Information movie S3). It took over an hour for actomyosin to deplete the released ATP molecules; therefore, it is necessary to remove the released ATP for the repeated release of ATP. For quick ATP consumption, we added 0.24 units·mL^{-1} hexokinase to the motility solution.[6,7] Hexokinase catalyzes ATP hydrolysis in the presence of glucose, and thus the ATP concentration in the flow cell was rapidly decreased by hexokinase. At first, when −1 V was applied to the graphene–polymer hybrid device for 3 s, actin filaments began to move. As the ATP molecules diffused from the PPy-ATP pattern, the speed of actin filaments was increased for a while. After that, the speed of actin filaments was decreased. Then actin filaments stopped because hexokinase depleted the released ATP. As shown in Supporting Information movie S3, actin filaments became short as time goes by. In this experiment, because hexokinase consumed the released ATP, the ATP concentration was not enough to activate all myosin on the graphene–polymer hybrid device. Therefore, actin filaments were broken by unactivated myosin over time.[45] After −3 V was applied to the device for 3 s, the actin filaments began to move again. We would like to point out that the actomyosin was repeatedly activated in real-time by electrical stimuli.

CONCLUSIONS

In conclusion, we report a strategy to control the transportation of actin filaments propelled by motor proteins in real-time using a graphene–polymer hybrid nanostructure as an integrated bioenergy storage device. Using the functionalized graphene, we successfully performed an *in vitro* motility assay on the graphene surface. PPy-ATP patterns were fabricated and aligned onto a desired location on the functionalized graphene and utilized as bioenergy containers for motor protein. ATP molecules were released from PPy-ATP patterns by electrical stimuli through the graphene substrates, which turned on the motility of the motor protein. Interestingly, the response of the graphene–polymer hybrid device could be regulated by controlling the viscosity of the surrounding media. Furthermore, we also demonstrated the repeated activation and deactivation of protein motors using the media with hexokinase, which depleted extra ATP. This built-in energy storage system can enable the local activation of motor protein with on/off switching, which should be useful for the applications requiring the sequential activation of multiple steps such as a motor-protein-based biosensor.[46] In addition, by combining our devices with previous motility control methods such as tracks for control of the sliding direction, widely spaced open zones for motility,[47] rectifiers,[48,49] and use of cytoskeletal filaments as shuttles,[50–53] one should be able to open up many new practical applications such as devices for controlled transfer of cargoes between different compartments in lab-on-a-chip applications. Thus, this hybrid platform can be a major breakthrough toward bioinspired nanomechanical systems.

MATERIALS AND METHODS

Fabrication of PPy-ATP Patterns on Functionalized Graphene. Multilayered graphene grown by a CVD method was transferred onto an oxygen plasma-cleaned cover glass as described previously.[54–56] The transferred graphene substrate was placed in a 1-pyrenebutylamine solution (1 mM in dimethyl sulfoxide) for 8 h, rinsed with ethanol, and then dried in a nitrogen gas flow. A Ti/Au (100/300 Å) electrode was fabricated on the graphene substrate *via* thermal evaporation through a shadow mask. After patterning AZ5214 photoresist *via* photolithography, PPy-ATP films were synthesized from the mixture of 0.1 M pyrrole and 20 mM ATP in an aqueous solution at +0.8 V (*vs* a Ag/AgCl reference electrode) using the electrochemical deposition method.[20] The ATP–pyrrole solution was kept at 4 °C during the deposition process. The photoresist pattern was utilized as a passivation layer, and therefore, PPy-ATP films were deposited only on the uncovered graphene surface. After then, the photoresist was removed by acetone, and the substrate was rinsed several times with acetone and deionized water. The substrate was placed in deionized water for 10 min to remove weakly bound ATP molecules on the surface of PPy-ATP patterns and then dried in nitrogen gas flow. The PPy-ATP film thickness measured by atomic force microscopy (AFM) was about 1 μm. Note that, since this patterning process is based on photolithography, it can be utilized to generate various nano- and microscale patterns over large surface area.[57]

***In Vitro* Motility Assay.** Actin and myosin were extracted from rabbit skeletal muscle. Myosin was digested to be utilized in forms of heavy meromyosin (HMM) by the method as described by Kron *et al.*[29] Actin filaments were stabilized and labeled with

tetramethylrhodamine phalloidin (adsorption maximum wavelength = 540 nm, emission maximum wavelength = 565 nm, R415, Invitrogen). For the motility assay on the functionalized graphene surfaces, the flow cell was constructed with scotch double-sided tapes and a cover glass. The flow cells were first incubated with 1 mg·mL^{-1} HMM for 3 min, 0.75 mg·mL^{-1} bovine serum albumin (BSA), and 2 μg·mL^{-1} labeled actin filaments infused into the flow cell in sequence and incubated in the flow cell for 1 min. Actin buffer (AB) (25 mM imidazole pH 7.4, 25 mM KCl, 4 mM $MgCl_2$, 1 mM EGTA, 1 mM dithiothreitol (DTT)) was infused to wash the flow cell between each step. Unlabeled actin filaments were not used to passivate dead myosin in this experiment, unlike the conventional *in vitro* motility assay,[23] because the residual unlabeled actin filaments could result in unexpected ATP consumption. Finally, the motility solution (3 mg·mL^{-1} D-glucose, 50 units·mL^{-1} glucose oxidase, 52 units·mL^{-1} catalase, 2 mM ATP in AB buffer) with 0.3% MC was infused to the flow cell, and the motility of labeled actin filaments was observed through the transparent graphene substrates *via* a fluorescent microscope.

For the real-time controlled motility assay using a graphene–polymer hybrid device, a flow cell was constructed with scotch double-sided tapes and a Ti/Au (100/300 Å) evaporated cover slide as a spacer and a counter electrode, respectively. We used the two-electrode system because the flow cell was too small to use the reference electrode.[58] The *in vitro* motility procedure was the same as described above except the motility solution (3 mg·mL^{-1} D-glucose, 50 units·mL^{-1} glucose oxidase, 52 units·mL^{-1} catalase in AB buffer) with the different concentration of MC. The flow-cell temperature was kept at 30 °C throughout all of our experiments except a temperature-controlled experiment. The temperature was controlled using an incubation system for microscope (Tokai Hit Co., Ltd.).

Bioluminescence Assay. We used a bioluminescence assay kit purchased from Sigma-Aldrich. A 25-fold dilution of ATP assay mix stock solution was used. The flow cell of a graphene–polymer hybrid device was constructed with scotch double-sided tapes and a Ti/Au (100/300 Å) evaporated cover slide as a spacer and a counter electrode, respectively. The ATP assay mix stock solution was infused into the flow cell, and then the negative bias voltage (−2 V *vs* the counter electrode) was repeatedly applied to the flow cell. The luminescence from the reaction was observed *via* fluorescence microscopy at a FITC channel.

Optical Imaging and Image Processing. Actomyosin motility in the flow cell was observed *via* a fluorescent microscope (Nikon, TE2000U) equipped with an EMCCD (Nikon, DQC FS) and a LED light source (Custom Interconnect Ltd., CoolLED). CoolLED pE-1 excitation system (Custom Interconnect Ltd., CoolLED) with excitation at 550 nm and a TRITC filter (Nikon, EX 540/25, DM 565, BA 605/55) were used for fluorescence imaging. We analyzed the trajectories of actin filaments using Metamorph analysis software (Molecular Devices).

Acknowledgment. This work was supported by the International Research & Development program of NRF funded by MEST of Korea (No. 2011-00240) and the NRF grant (No. 2011-0000390). We thank Jai Hyun Koh and Kookheon Char in the School of Chemical & Biological Engineering at Seoul National University for helping us with the contact angle measurement. S.H. acknowledges the support from the Converging Research Center Program (No. 2011K000683).

Supporting Information Available: Supporting figures, supporting table, a supplementary note, and supporting movies. This material is available free of charge via the Internet at http://pubs.acs.org.

REFERENCES AND NOTES

1. Van den Heuvel, M. G. L.; Dekker, C. Motor Proteins at Work for Nanotechnology. *Science* **2007**, *317*, 333–336.
2. Agarwal, A.; Hess, H. Biomolecular Motors at the Intersection of Nanotechnology and Polymer Science. *Prog. Polym. Sci.* **2010**, *35*, 252–277.
3. Fulga, F.; Nicolau, D. V.; Nicolau, D. V. Models of Protein Linear Molecular Motors for Dynamic Nanodevices. *Integr. Biol.* **2009**, *1*, 150–169.
4. Yokokawa, R.; Takeuchi, S.; Kon, T.; Nishiura, M.; Ohkura, R.; Sutoh, K.; Fujita, H. Hybrid Nanotransport System by Biomolecular Linear Motors. *J. Microelectromech. Syst.* **2004**, *13*, 612–619.
5. Wasylycia, J. R.; Sapelnikova, S.; Jeong, H.; Dragoljic, J.; Marcus, S. L.; Harrison, D. J. Nano-biopower Supplies for Biomolecular Motors: The Use of Metabolic Pathway-Based Fuel Generating Systems in Microfluidic Devices. *Lab Chip* **2008**, *8*, 979–982.
6. Liu, H. Q.; Schmidt, J. J.; Bachand, G. D.; Rizk, S. S.; Looger, L. L.; Hellinga, H. W.; Montemagno, C. D. Control of a Biomolecular Motor-Powered Nanodevice with an Engineered Chemical Switch. *Nat. Mater.* **2002**, *1*, 173–177.
7. Greene, A. C.; Trent, A. M.; Bachand, G. D. Controlling Kinesin Motor Proteins in Nanoengineered Systems through a Metal-Binding On/Off Switch. *Biotechnol. Bioeng.* **2008**, *101*, 478–486.
8. Hess, H.; Clemmens, J.; Qin, D.; Howard, J.; Vogel, V. Light-Controlled Molecular Shuttles Made from Motor Proteins carrying Cargo on Engineered Surfaces. *Nano Lett.* **2001**, *1*, 235–239.
9. Tucker, R.; Katira, P.; Hess, H. Herding Nanotransporters: Localized Activation *via* Release and Sequestration of Control Molecules. *Nano Lett.* **2008**, *8*, 221–226.
10. Nomura, A.; Uyeda, T. Q. P.; Yumoto, N.; Tatsu, Y. Photo-Control of Kinesin-Microtubule Motility Using Caged Peptides Derived from the Kinesin C-Terminus Domain. *Chem. Commun.* **2006**, 3588–3590.
11. Mihajlovic, G.; Brunet, N. M.; Trbovic, J.; Xiong, P.; Von Molnar, S.; Chase, P. B. All-Electrical Switching and Control Mechanism for Actomyosin-Powered Nanoactuators. *Appl. Phys. Lett.* **2004**, *85*, 1060–1062.
12. Martin, B. D.; Velea, L. M.; Soto, C. M.; Whitaker, C. M.; Gaber, B. P.; Ratna, B. Reversible Control of Kinesin Activity and Microtubule Gliding Speeds by Switching the Doping States of a Conducting Polymer Support. *Nanotechnology* **2007**, *18*, 055103–055109.
13. Dujovne, I.; Van den Heuvel, M.; Shen, Y.; De Graaff, M.; Dekker, C. Velocity Modulation of Microtubules in Electric Fields. *Nano Lett.* **2008**, *8*, 4217–4220.
14. Riveline, D.; Ott, A.; Julicher, F.; Winkelmann, D. A.; Cardoso, O.; Lacapere, J. J.; Magnusdottir, S.; Viovy, J. L.; Gorre-Talini, L.; Prost, J.; *et al.* Acting on Actin: The Electric Motility Assay. *Eur. Biophys. J. Biophys.* **1998**, *27*, 403–408.
15. Mohanty, N.; Berry, V. Graphene-Based Single-Bacterium Resolution Biodevice and DNA Transistor: Interfacing Graphene Derivatives with Nanoscale and Microscale Biocomponents. *Nano Lett.* **2008**, *8*, 4469–4476.
16. Ang, P. K.; Jaiswal, M.; Lim, C. H. Y. X.; Wang, Y.; Sankaran, J.; Li, A.; Lim, C. T.; Wohland, T.; Barbaros, O.; Loh, K. P.; *et al.* A Bioelectronic Platform Using a Graphene–Lipid Bilayer Interface. *ACS Nano* **2010**, *4*, 7387–7394.
17. Bae, S.; Kim, H.; Lee, Y.; Xu, X. F.; Park, J. S.; Zheng, Y.; Balakrishnan, J.; Lei, T.; Kim, H. R.; Song, Y. I.; *et al.* Roll-to-Roll Production of 30-in. Graphene Films for Transparent Electrodes. *Nat. Nanotechnol.* **2010**, *5*, 574–578.
18. Wang, X.; Zhi, L. J.; Mullen, K. Transparent, Conductive Graphene Electrodes for Dye-Sensitized Solar Cells. *Nano Lett.* **2008**, *8*, 323–327.
19. Guimard, N. K.; Gomez, N.; Schmidt, C. E. Conducting Polymers in Biomedical Engineering. *Prog. Polym. Sci.* **2007**, *32*, 876–921.
20. Pyo, M.; Maeder, G.; Kennedy, R. T.; Reynolds, J. R. Controlled-Release of Biological Molecules from Conducting Polymer-Modified Electrodes: The Potential-Dependent Release of Adenosine 5′-Triphosphate from Poly(pyrrole adenosine 5′-triphosphate) Films. *J. Electroanal. Chem.* **1994**, *368*, 329–332.
21. Pyo, M.; Reynolds, J. R. Electrochemically Stimulated Adenosine 5′-Triphosphate (ATP) Release through Redox Switching of Conducting Polypyrrole Films and Bilayers. *Chem. Mater.* **1996**, *8*, 128–133.
22. Li, L. D.; Huang, C. B. Electrochemical/Electrospray Mass Spectrometric Studies of Electrochemically Stimulated ATP Release from PP/ATP Films. *J. Am. Soc. Mass. Spectrom.* **2007**, *18*, 919–926.

23. Ge, D. T.; Tian, X. D.; Qi, R.; Huang, S. Q.; Mu, J.; Hong, S. M.; Ye, S. F.; Zhang, X. M.; Li, D. H.; Shi, W.; *et al.* A Polypyrrole-Based Microchip for Controlled Drug Release. *Electrochim. Acta* **2009**, *55*, 271–275.
24. Schmidt, C. E.; Shastri, V. R.; Vacanti, J. P.; Langer, R. Stimulation of Neurite Outgrowth Using an Electrically Conducting Polymer. *Proc. Natl. Acad. Sci. U.S.A.* **1997**, *94*, 8948–8953.
25. Aizawa, M.; Haruyama, T.; Khan, G. F.; Kobatake, E.; Ikariyama, Y. Electronically Modulated Biological Functions of Molecular Interfaced Enzymes and Living Cells. *Biosens. Bioelectron.* **1994**, *9*, 601–610.
26. Wang, X. R.; Tabakman, S. M.; Dai, H. J. Atomic Layer Deposition of Metal Oxides on Pristine and Functionalized Graphene. *J. Am. Chem. Soc.* **2008**, *130*, 8152.
27. An, X.; Simmons, T.; Shah, R.; Wolfe, C.; Lewis, K. M.; Washington, M.; Nayak, S. K.; Talapatra, S.; Kar, S. Stable Aqueous Dispersions of Noncovalently Functionalized Graphene from Graphite and Their Multifunctional High-Performance Applications. *Nano Lett.* **2010**, *10*, 4295–4301.
28. Vale, R. D.; Milligan, R. A. The Way Things Move: Looking under the Hood of Molecular Motor Proteins. *Science* **2000**, *288*, 88–95.
29. Kron, S. J.; Toyoshima, Y. Y.; Uyeda, T. Q. P.; Spudich, J. A. Assays for Actin Sliding Movement over Myosin-Coated Surfaces. *Methods Enzymol.* **1991**, *196*, 399–416.
30. Nair, R. R.; Blake, P.; Grigorenko, A. N.; Novoselov, K. S.; Booth, T. J.; Stauber, T.; Peres, N. M. R.; Geim, A. K. Fine Structure Constant Defines Visual Transparency of Graphene. *Science* **2008**, *320*, 1308–1308.
31. Byun, K. E.; Kim, M. G.; Chase, P. B.; Hong, S. H. Selective Assembly and Guiding of Actomyosin Using Carbon Nanotube Network Monolayer Patterns. *Langmuir* **2007**, *23*, 9535–9539.
32. Zhang, H.; Lamb, R.; Lewis, J. Engineering Nanoscale Roughness on Hydrophobic Surface: Preliminary Assessment of Fouling Behaviour. *Sci. Technol. Adv. Mater.* **2005**, *6*, 236–239.
33. Leroy, F.; Muller-Plathe, F. Rationalization of the Behavior of Solid−Liquid Surface Free Energy of Water in Cassie and Wenzel Wetting States on Rugged Solid Surfaces at the Nanometer Scale. *Langmuir* **2011**, *27*, 637–645.
34. Koc, Y.; De Mello, A. J.; McHale, G.; Newton, M. I.; Roach, P.; Shirtcliffe, N. J. Nano-scale Superhydrophobicity: Suppression of Protein Adsorption and Promotion of Flow-Induced Detachment. *Lab Chip* **2008**, *8*, 582–586.
35. Albet-Torres, N.; O'Mahony, J.; Charlton, C.; Balaz, M.; Lisboa, P.; Aastrup, T.; Mansson, A.; Nicholls, I. A. Mode of Heavy Meromyosin Adsorption and Motor Function Correlated with Surface Hydrophobicity and Charge. *Langmuir* **2007**, *23*, 11147–11156.
36. Albet-Torres, N.; Gunnarsson, A.; Persson, M.; Balaz, M.; Hook, F.; Mansson, A. Molecular Motors on Lipid Bilayers and Silicon Dioxide: Different Driving Forces for Adsorption. *Soft Matter* **2010**, *6*, 3211–3219.
37. Nicolau, D. V.; Solana, G.; Kekic, M.; Fulga, F.; Mahanivong, C.; Wright, J.; Dos Remedios, C. G. Surface Hydrophobicity Modulates the Operation of Actomyosin-Based Dynamic Nanodevices. *Langmuir* **2007**, *23*, 10846–10854.
38. Jaber, J. A.; Chase, P. B.; Schlenoff, J. B. Actomyosin-Driven Motility on Patterned Polyelectrolyte Mono- and Multilayers. *Nano Lett.* **2003**, *3*, 1505–1509.
39. Siepmann, J.; Ainaoui, A.; Vergnaud, J. M.; Bodmeier, R. Calculation of the Dimensions of Drug−Polymer Devices Based on Diffusion Parameters. *J. Pharm. Sci.* **1998**, *87*, 827–832.
40. Sun, P.; Laforge, F. O.; Mirkin, M. V. Scanning Electrochemical Microscopy in the 21st Century. *Phys. Chem. Chem. Phys.* **2007**, *9*, 802–823.
41. Kron, S. J.; Spudich, J. A. Fluorescent Actin-Filaments Move on Myosin Fixed to a Glass-Surface. *Proc. Natl. Acad. Sci. U.S.A.* **1986**, *83*, 6272–6276.
42. *Mechanics of Motor Proteins and the Cytoskeleton*; Howard, J., Ed.; Sinauer Associates: Sunderland, MA, 2001; p 367.
43. Siepmann, J.; Lecomte, F.; Bodmeier, R. Diffusion-Controlled Drug Delivery Systems: Calculation of the Required Composition To Achieve Desired Release Profiles. *J. Controlled Release* **1999**, *60*, 379–389.
44. Harada, Y.; Sakurada, K.; Aoki, T.; Thomas, D. D.; Yanagida, T. Mechanochemical Coupling in Actomyosin Energy Transduction Studied by *In-Vitro* Movement Assay. *J. Mol. Biol.* **1990**, *216*, 49–68.
45. Homsher, E.; Wang, F.; Sellers, J. R. Factors Affecting Movement of F-Actin Filaments Propelled by Skeletal-Muscle Heavy-Meromyosin. *Am. J. Physiol.* **1992**, *262*, C714–C723.
46. Fischer, T.; Agarwal, A.; Hess, H. A Smart Dust Biosensor Powered by Kinesin Motors. *Nat. Nanotechnol.* **2009**, *4*, 162–166.45.
47. Bunk, R.; Sundberg, M.; Mansson, A.; Nicholls, I. A.; Omling, P.; Tagerud, S.; Montelius, L. Guiding Motor-Propelled Molecules with Nanoscale Precision through Silanized Bi-channel Structures. *Nanotechnology* **2005**, *16*, 710.
48. Hiratsuka, Y.; Tada, T.; Oiwa, K.; Kanayama, T.; Uyeda, T. Q. P. Controlling the Direction of Kinesin-Driven Microtubule Movements along Microlithographic Tracks. *Biophys. J.* **2001**, *81*, 1555–1561.
49. Van den Heuvel, M. G. L.; Butcher, C. T.; Smeets, R. M. M.; Diez, S.; Dekker, C. High Rectifying Efficiencies of Microtubule Motility on Kinesin-Coated Gold Nanostructures. *Nano Lett.* **2005**, *5*, 1117–1122.
50. Mansson, A.; Sundberg, M.; Balaz, M.; Bunk, R.; Nicholls, I. A.; Omling, P.; Tagerud, S.; Montelius, L. *In Vitro* Sliding of Actin Filaments Labelled with Single Qantum Dots. *Biochem. Biophys. Res. Commun.* **2004**, *314*, 529–534.
51. Brunner, C.; Wahnes, C.; Vogel, V. Cargo Pick-Up from Engineered Loading Stations by Kinesin Driven Molecular Shuttles. *Lab Chip* **2007**, *7*, 1263–1271.
52. Hiyama, S.; Gojo, R.; Shima, T.; Takeuchi, S.; Sutoh, K. Biomolecular-Motor-Based Nano- or Microscale Particle Translocations on DNA Microarrays. *Nano Lett.* **2009**, *9*, 2407–2413.
53. Takatsuki, H.; Tanaka, H.; Rice, K. M.; Kolli, M. B.; Nalabotu, S. K.; Kohama, K.; Famouri, P.; Blough, E. R. Transport of Single Cells Using an Actin Bundle-Myosin Bionanomotor Transport System. *Nanotechnology* **2011**, *22*, 245101.
54. Jeon, I.; Yang, H.; Lee, S.-H.; Heo, J.; Seo, D. H.; Shin, J.; Chung, U. I.; Kim, Z. G.; Chung, H. J.; Seo, S.; *et al.* Passivation of Metal Surface States: Microscopic Origin for Uniform Monolayer Graphene by Low Temperature Chemical Vapor Deposition. *ACS Nano* **2011**, *5*, 1915–20.
55. Kim, K. S.; Zhao, Y.; Jang, H.; Lee, S. Y.; Kim, J. M.; Kim, K. S.; Ahn, J. H.; Kim, P.; Choi, J. Y.; Hong, B. H.; *et al.* Large-Scale Pattern Growth of Graphene Films for Stretchable Transparent Electrodes. *Nature* **2009**, *457*, 706–710.
56. Reina, A.; Jia, X. T.; Ho, J.; Nezich, D.; Son, H. B.; Bulovic, V.; Dresselhaus, M. S.; Kong, J. Large Area, Few-Layer Graphene Films on Arbitrary Substrates by Chemical Vapor Deposition. *Nano Lett.* **2009**, *9*, 30–35.
57. Pease, R. F.; Chou, S. Y. Lithography and Other Patterning Techniques for Future Electronics. *Proc. IEEE* **2008**, *96*, 248–270.
58. Van den Heuvel, M. G. L.; Butcher, C. T.; Lemay, S. G.; Diez, S.; Dekker, C. Electrical Docking of Microtubules for Kinesin-Driven Motility in Nanostructures. *Nano Lett.* **2005**, *5*, 235–241.